

Estimating Black Carbon Concentration from Urban Traffic Using Vision-Based Machine Learning

Camellia Zakaria

University of Toronto
Canada

camellia.zakaria@utoronto.ca

Aryan Sadeghi

University of Toronto
Canada

aryan.sadeghi@utoronto.ca

Weaam Jaafar

University of Toronto
Canada

weaam.jaafar@mail.utoronto.ca

Junshi Xu

University of Hong Kong
Hong Kong

junshixu@hku.hk

Alex Mariakakis

University of Toronto
Canada

alex.mariakakis@utoronto.ca

Marianne Hatzopoulou

University of Toronto
Canada

marianne.hatzopoulou@utoronto.ca

Abstract

Black carbon (BC) emissions in urban areas are primarily driven by traffic, with hotspots near major roads disproportionately affecting marginalized communities. Because BC monitoring is typically performed using costly and specialized instruments, there is little to no available data on BC concentration from local traffic sources that could help inform policy interventions targeting local factors. By contrast, traffic monitoring systems are widely deployed in cities around the world, highlighting the imbalance between what we know about traffic conditions and what we do not know about their environmental consequences. To bridge this gap, we propose a machine learning-driven system that extracts visual information from traffic video to capture vehicle behaviors and conditions. Combining these features with weather data, our model estimates BC at street level, achieving an R^2 of 0.72 and RMSE of 129.42 ng/m^3 . From a sustainability perspective, this work leverages resources already supported by urban infrastructure and established modeling techniques to generate information relevant to traffic emission. Obtaining BC concentration data provides actionable insights to support pollution reduction, urban planning, public health, and environmental justice at the local municipal level.

Permission to make digital or hard copies of all or part of this work for personal or classroom use is granted without fee provided that copies are not made or distributed for profit or commercial advantage and that copies bear this notice and the full citation on the first page. Copyrights for components of this work owned by others than the author(s) must be honored. Abstracting with credit is permitted. To copy otherwise, or republish, to post on servers or to redistribute to lists, requires prior specific permission and/or a fee. Request permissions from permissions@acm.org. *MobiSys '26*, XXX, XXX, XXX

© 2025 Copyright held by the owner/author(s). Publication rights licensed to ACM.

ACM ISBN 978-x-xxxx-xxxx-x/YYYY/MM

<https://doi.org/XXXXXXX.XXXXXXX>

CCS Concepts

• **Computing methodologies** → **Computer vision**; **Supervised learning by regression**; • **Human-centered computing** → **Empirical studies in ubiquitous and mobile computing**; • **Applied computing** → **Health informatics**.

Keywords

black carbon, traffic pollution, environmental justice, computer vision, machine learning, prototype implementation

ACM Reference Format:

Camellia Zakaria, Aryan Sadeghi, Weaam Jaafar, Junshi Xu, Alex Mariakakis, and Marianne Hatzopoulou. 2025. Estimating Black Carbon Concentration from Urban Traffic Using Vision-Based Machine Learning. In *Proceedings of 24th ACM International Conference on Mobile Systems, Applications, and Services (MobiSys '26)*. ACM, New York, NY, USA, 18 pages. <https://doi.org/XXXXXXX.XXXXXXX>

1 Introduction

Black carbon (BC) is produced from the incomplete combustion of fossil fuels, biomass, and biofuels. High exposures to BC adversely affect human health by increasing the risks of asthma, cardiovascular disease, and premature death in vulnerable populations (e.g., children, the elderly, and those with preexisting conditions) [42]. As a short-lived climate pollutant (SLCP), BC contributes to rapid warming but remains in the atmosphere for only days to decades, unlike long-lived gases such as carbon dioxide. Reducing BC, among other SLCPs, offers a way to slow global warming quickly while delivering substantial air quality and health benefits [15].

Although BC emissions are primarily generated from household solid fuel use and open biomass burning, vehicle emissions are a significant contributor in urban areas

[17, 41]. In large cities such as Toronto, hotspots are located primarily near major roads, highways, and freight distribution centers adjacent to socially disadvantaged neighborhoods [39]. Despite its considerable effects on human and environmental health, data on BC pollution from traffic activities remain far less accessible to the public than data on other common pollutants such as carbon dioxide [5]. Environmental research studies related to vehicle-based BC emissions have identified the speed and type of vehicles as key local factors, ignoring complications attributed to spatial-temporal variability on urban and regional scales [10, 41]. Specifically, urban structures and environmental factors, such as wind speed and humidity, influence particle accumulation.

BC is typically measured using mobile air quality monitoring systems. These systems utilize Google Street View cars, with photoacoustic spectrometers [24] or optical microaethalometers [22, 37, 39] to measure pollutant concentrations. The potential for pervasive monitoring with these instruments is due to their prohibitive costs. BC concentration data from vehicles is also inaccessible because manufacturers use proprietary protocols, offering little to no publicly available data standard. Conversely, intelligent transportation systems focus largely on traffic management, vehicle and driver behavior, and road safety solutions [1]; thus, it highlights a critical gap between abundant traffic surveillance data and the scarcity of traffic emission data.

This data gap motivates our exploration of alternative methods to estimate BC concentrations from traffic data. We hypothesize that *traffic feeds can serve as a viable data source to approximate BC concentration in urban traffic conditions*. Specifically, we pose the following research questions:

- RQ1.** How accurately can a machine learning model trained on video-derived traffic features estimate BC concentrations?
- RQ2.** What video-derived traffic features are most predictive of local BC concentrations?
- RQ3.** Under what conditions and for what reasons does the model perform poorly across traffic scenarios?

Using a data collection platform that automatically integrates traffic video streams with environmental data, we conducted a field study along several common roads along Downtown Toronto to collect BC concentration readings using a microaethalometer for ground truth. We analyzed the resulting dataset with well-established computer vision (CV) models to extract characteristics of vehicle emission covariates (i.e., vehicle type, vehicle count, stop and accelerate behaviors on different lanes) under varying traffic conditions. Having video-derived features and API-based information from traffic and environmental data as input, we built a machine learning model to estimate BC

concentrations at 30-second intervals. Our results from evaluating an XGBoost regression model yield strong predictive performance ($\text{RMSE} = 129.42 \text{ ng/m}^3$, $R^2=0.72$), with vehicle acceleration, vehicle distance from the microaethalometer and wind speed being the most significant predictors. These findings are consistent with previous findings that BC is concentrated near the emission origin and decreases with distance.

Our implementation highlights the technical feasibility of leveraging traffic video recording and established CV techniques to accurately determine a set of vehicle emission covariates as significant predictors of approximating BC concentrations in traffic situations. However, our work clearly requires longitudinal data collection to capture seasonal variations. It should be emphasized that the focus of this study is on the detection framework itself, which encompasses the development of our data collection platform and techniques for feature extraction and modeling. This approach is not intended to replace high-precision microaethalometers, as they remain necessary to provide ground-truth measurements. Nonetheless, by continuing to use traffic data in novel ways, we can move beyond traffic monitoring insights to inform end-users of health-related information. From a sustainability perspective, this work rests on two key ideas:

- (1) It builds on robust field-tested machine learning methods that form the backbone of deployed traffic safety systems and common urban technologies.
- (2) Using widely available infrastructure and abundant traffic feed data, it enables cities to address data gaps that cannot afford dedicated equipment.

While some location-specific calibration using limited ground-truth measurements may be necessary, this requirement is far less costly than deploying a full sensor network, making the approach practical and scalable. Thus, our research directly supports the United Nations Sustainable Development Goals [2]. The fine-scale spatial and temporal variability of BC emissions makes it a particularly relevant metric for assessing intra-urban disparities in exposure [19, 32, 34]. At the same time, marginalized and low-income communities are often located near high-traffic environments and industrial corridors, resulting in disproportionate exposure burdens. Our work enables both forward-looking projections and retrospective analyses, making the data more versatile to guide city planning, policy interventions, and public health measures [4, 28]. In doing so, our efforts aim to reduce the disproportionate burden on disadvantaged communities (SDG 10), inform sustainable urban development (SDG 11) and population health (SDG 3), and accelerate climate action by targeting SLCPs (SDG 13).

We extend the impact of our work by providing our data collection system, dataset, and models as publicly available resources via <https://github.com/sensAILabs/BCTraffic>. Descriptions of these resources are also in the Appendix.

2 Related Work

We review work on vehicle-related emissions, the environmental factors that influence them, and estimation methods for BC concentration, including ML approaches.

2.1 Data Collection for Black Carbon

Portable instruments on mobile platforms are often utilized to characterize this spatiotemporal variability and the actual levels of BC [37]. Measurement of BC concentration requires optical analyzers such as a microaethalometer, which measures the attenuation of an 880-nanometer radiation beam transmitted through a filter strip [22]. The device costs approximately USD\$6,000 and requires expert knowledge. Such device inaccessibility has led to significant amounts of missing data in BC reporting and hinders public health education and the development of evidence-based environmental policies. For example, the Canada Air Pollutant Emissions Inventory (APEI) approximates the BC concentration resulting from Transportation and Mobile Equipment through air transportation, domestic marine navigation, fishing and military, and rail transportation reporting [14]. These reports do not include elements with which the general public is likely to encounter or engage, such as those from on-road vehicles in urban and suburban traffic conditions. In addition, individual vehicle manufacturers have a bespoke testing protocol; specifically, manufacturers report the total particulate mass from which BC must be inferred indirectly [35].

2.2 Emissions from Local Vehicle Sources

Research has reported increasing concerns about the negative impacts of transportation on BC pollution. Specifically, near-road air quality in urban areas can fluctuate significantly over short distances and time frames [30]. BC concentration is strongly influenced by vehicle type, speed, and traffic density. A study by Zheng *et al.* measured BC concentration from eight light-duty passenger vehicles (LDPVs) with different engine technologies using a dynamometer and a microaethalometer (the same BC device we utilized for our study). The results showed that the BC emission factors varied significantly depending on the vehicle type and its engine. Diesel engines emitted between 3.6 to 91.5 mg/km, gasoline direct injection (GDI) engines produced 7.6 mg/km, and gasoline port-fuel injection (PFI) engines had the lowest emission rates, ranging from 0.13 to 0.58 mg/km [47]. Gasoline PFI vehicles exhibited peak BC

emissions during cold starts and aggressive high-speed driving, which contributed to elevated ambient BC concentrations. On the other hand, heavy-duty vehicles (HDVs) such as buses and trucks contributed disproportionately to both emissions and concentration levels [46]. The influence of vehicle speed should be considered along with vehicle type [3]. At very low speeds (30 km/h), common in urban congestion, BC emissions tend to be high due to frequent stop-and-go driving, leading to incomplete fuel combustion due to frequent acceleration and deceleration [10, 46]. At higher speeds (50–70 km/h), emissions tend to be lower, as combustion is more efficient under steady driving conditions. Large cities like Toronto and Montreal are predominantly characterized by clusters of BC sources concentrated around transportation infrastructure and dense urban cores [4]. Suburban areas, on the other hand, while generally experiencing lower overall traffic volumes, can exhibit higher per capita emissions due to a greater reliance on personal vehicles and a more limited access to public transportation options.

2.3 Traffic Air Pollution Mobile Monitoring

Mobile setups for outdoor air quality monitoring systems typically consist of Google Street View cars as the mobile sampling platform, and are equipped with 1-Hz instruments (e.g., gas analyzers) to measure the concentrations of pollutants [24]. Several studies aimed to understand BC pollution in different cities, such as Cairo, Shanghai and Toronto, employed microaethalometer (AE51, AethLabs) for BC data collection [22, 37, 39]. Generally, BC measurements are challenging because they are influenced by spatial-temporal variability on the *local*, *urban*, and *regional* scales [41]. In the example of near-road air quality, BC amounts are determined by attributes of local sources (e.g., emission from a truck differs from a bus) and impacts of wind speed and humidity from local and nearby regions.

Using Land Use Regression, this method uses environmental data to identify how different land uses influence BC concentration. Recent studies reported that ML models, such as Random Forests [21] and Kernel-based Regularized Least Squares [43], outperform traditional regression models in capturing complex nonlinear relationships related to the built environment. Separately, studies on vehicle identification have proposed CV techniques, implemented with deep learning (DL) models to predict vehicle speed using traffic surveillance [18], vehicle type using sound [8], and improved detections under varying weather conditions using LiDAR [31]. However, such analysis is based on static features of the built environment. Our goal is to incorporate real-time vehicle behaviors and conditions that directly drive emissions.

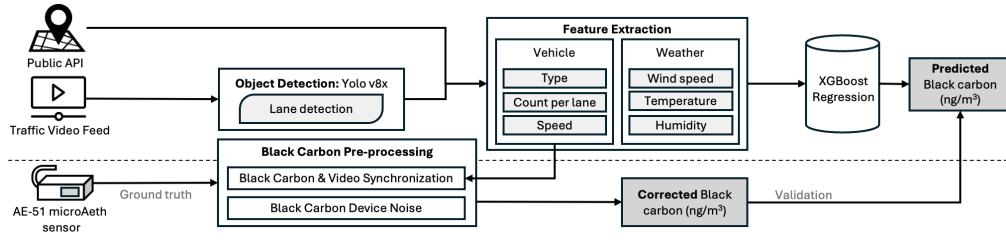


Figure 1: End-to-end system overview for BC estimation with computer vision and machine learning techniques.

2.4 Why Traffic Video Feeds?

Air quality analysis typically relies on a combination of regulatory-grade monitoring stations, which provide high accuracy. A single regulatory-grade station can cost in the range of several hundred thousand dollars to install and maintain, making pervasive coverage across cities or rural areas impractical. Low-cost fixed sensors and mobile sensing platforms can complement fixed setups. However, a study by deSouza *et al.* on the distribution of low-cost air quality sensors within the U.S. reported these sensors were more available in higher-income, predominantly White areas [9]. At the same time, CNBC estimated over 770 million surveillance cameras installed worldwide, with 18% located in the Americas and 54% concentrated in China [33]. Today, nearly every major city has invested in intelligent traffic management or law enforcement surveillance, with cameras and sensors continuously generating vast data streams. These systems undeniably provide powerful capabilities for monitoring and regulating traffic violations and driver behavior. However, the disproportionately higher deployments of surveillance cameras in low-income neighborhoods under the banner of traffic and community safety have raised important equity concerns [36]. The abundance of traffic cameras, while enhancing safety and enforcement, not only raises equity concerns but also highlights a critical gap. Data on traffic-related emissions remain scarce [1]. This disconnect prompts a critical question: **How can traffic data already available in the environment draw inferences about black carbon concentration from traffic?**

Key Takeaway: Collectively, these reports support our direction to explore traffic video data as a potential source, as many environmental studies rely on a fixed set of vehicle emission covariates we believe can be captured using CV techniques. First, *stop-and-go* conditions are most evident during periods of heavy traffic congestion. Second, *heavy-duty vehicles* have a disproportionate impact and short spikes are strongly influenced by vehicle states such as idling and acceleration. Environmental features also

matter at short time scales: *wind speed* influences local concentration. Although CV and ML research has advanced many areas of traffic monitoring and surveillance, prior work has not examined how the infrastructure and techniques can be used to predict BC from traffic.

3 Proposed System

Figure 1 illustrates the overview of our proposed system. We estimate key vehicular emission covariates by applying CV techniques to analyze traffic video recordings and extract local factors (i.e., vehicle and traffic-related characteristics). These features are used to approximate BC concentration as measured by a microaethalometer.

3.1 Video-Derived Vehicle Features

We extract vehicle-related information from video data using a pre-trained YOLOv8 model [40], which is able to accurately determine vehicle characteristics (e.g., cars from trucks). However, extracting these vehicle emission covariates involves two non-trivial challenges. The first relates to distinguishing whether vehicles are closer or farther away from the deployed microaethalometer. The other requires determining a stop or idle as such actions emit high BC concentration when vehicles accelerate.

3.1.1 Assumptions. Several aspects of our implementation are based on underlying assumptions. First, the vehicle lanes in our dataset are relatively straight (see Figure 6 for street illustrations). Although established CV techniques can accommodate curved or non-linear lanes, ours does not adopt these complex approaches. Second, the camera placement limits our field of view, occasionally resulting in partial occlusion of full traffic flow. Standard traffic-surveillance setups do not face this constraint, and we mitigate this limitation by pulling traffic density and speed data from the TomTom API [38].

3.1.2 Detecting Vehicles by Lane. Our approach requires differentiating vehicles by traffic lanes, where vehicles along the first lane closest to our setup are expected to have the most direct impact on BC measurements. However, this

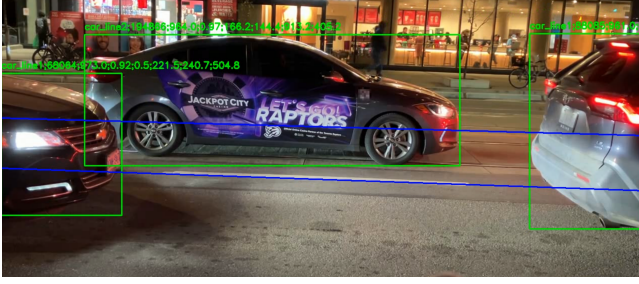


Figure 2: Result of applying YOLO and Hough Transform to determine the type of vehicle and distance from the microaethalometer.

capability is not inherently supported by YOLO. Hence, we use the Hough Transform, a well-established CV technique to detect straight lines [11]. As per Figure 2, it employs Canny Edge Detection to extract edges, producing lane lines frame-by-frame. Once the lanes are identified, each detected vehicle is assigned a lane by comparing the vehicle’s centroid in the boundary box with the lane boundary lines. This segmentation allows us to count vehicles in each lane separately.

3.1.3 Vehicle Stop-and-Idle and Count Estimation. To differentiate stopped or idle vehicles from those that only decelerate, we used a heuristically driven approach. First, we extended the vehicle detection module with a threshold-based method that analyzes motion across consecutive frames. By tracking positional shifts and estimating speed, we classify a vehicle as “stopped” if its speed remains near zero for at least four seconds. In addition, we incorporated traffic density and speed data from the TomTom API to help estimate vehicle counts and overall flow conditions, compensating for the limited field of view from our camera placement. Together, these heuristics allowed us to better distinguish stationary vehicles from those that simply moved slowly.

3.2 Black Carbon Pre-processing Module

Microaethalometers sample BC concentration at a fixed resolution of 10–30 seconds [25]. While we rely on this data as the ground truth for our models, we pre-process it to handle two key challenges: the presence of noise caused by faulty device calibration, and unsupported synchronization between the BC ground truth and extracted video features.

3.2.1 Challenge #1: Microaethalometer Data Noise. To preserve data integrity while minimizing the effect of noise, we apply the Optimized Noise-Reduction Algorithm (ONA), a filtering technique by Hagler *et al.* that applies adaptive time-averaging to BC readings, adjusting the averaging

window based on the incremental light attenuation detected by the instrument’s internal filter [16]. Separately, we remove outliers, data points that fall outside the 95% confidence interval. Our method distinguishes between global and local trimming; that is, local trimming preserves the unique distribution in each dataset, while global trimming applies the same criteria across all datasets.

3.2.2 Challenge #2: Synchronization between Black Carbon and Video Data. To address the temporal misalignment between BC ground truth data and current traffic density, we identified the optimal time shift that best aligns the two readings. Specifically, we transformed both signals into the frequency domain using the Discrete Fourier Transform (DFT), where time shifts are reflected as phase differences. Then, we computed the cosine similarity across varying phase offsets to determine the time shift that yielded the highest alignment. Specifically, let $x[n]$ and $y[n]$ represent the two signals. The DFT is applied to both signals, where $X[k]$ and $Y[k]$ are the representations of the frequency domain, j facilitates the representation of both magnitude and phase information of the signal components, and k indexes the discrete frequency components, as follows:

$$X[k] = \sum_{n=0}^{N-1} x[n]e^{-j2\pi \frac{kn}{N}}, \quad Y[k] = \sum_{n=0}^{N-1} y[n]e^{-j2\pi \frac{kn}{N}}$$

To identify the optimal time shift $\Delta t_{\text{optimal}}$, we compute the cosine similarity between the frequency domain representations for various shifts, where $\langle \mathbf{X}, \mathbf{Y} \rangle$ is the dot product of the cosine and sine waves of the DFT vectors and $\|\mathbf{X}\|$ and $\|\mathbf{Y}\|$ are their Euclidean norms.

$$\text{Cosine Similarity} = \frac{\langle \mathbf{X}, \mathbf{Y} \rangle}{\|\mathbf{X}\| \|\mathbf{Y}\|}$$

With the components separated as $X_{\cos} = \cos(X[k])$, $X_{\sin} = \sin(X[k])$, $Y_{\cos} = \cos(Y[k])$, $Y_{\sin} = \sin(Y[k])$, respectively, we compute the cosine similarity between these components as follows:

$$\text{Cosine Similarity} = \frac{\langle X_{\cos}, Y_{\cos} \rangle + \langle X_{\sin}, Y_{\sin} \rangle}{\sqrt{\|X_{\cos}\|^2 + \|X_{\sin}\|^2} \sqrt{\|Y_{\cos}\|^2 + \|Y_{\sin}\|^2}}$$

Where \mathcal{S} is the set of candidate shifts within a reasonable range, we experimentally test various time shifts to identify the most optimal shift, $\Delta t_{\text{optimal}}$, which maximizes the cosine similarity between the representations of the frequency domain, thus aligning the time domain signals.

$$\Delta t_{\text{optimal}} = \arg \max_{\Delta t \in \mathcal{S}} (\text{Cosine Similarity}(X[k], \mathcal{F}\{y[n - \Delta t]\}))$$

By applying this shift as shown in Figure 3, we achieved corrected BC-FFT signals that improve the alignment between BC data and vehicle activity, as shown in Figure 4.

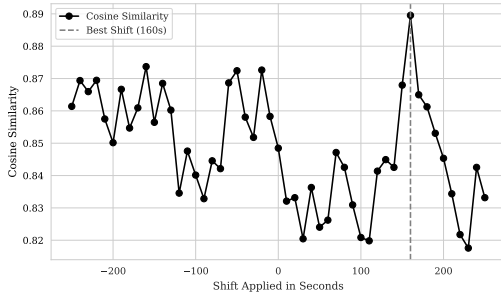


Figure 3: Cosine similarity between Fourier transformed BC vector and Fourier transformed *TotalVehicle* vector. The corrected BC signal is determined by the shift that maximizes cosine similarity (160 seconds).

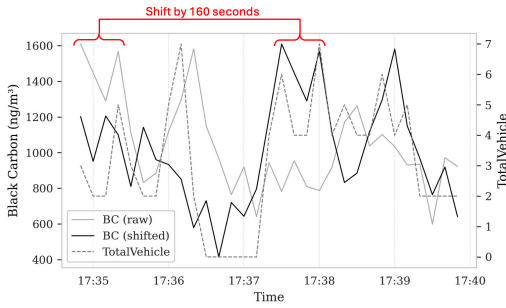


Figure 4: Original BC signal (gray) plotted alongside vehicle counts (dotted line) reveals a temporal misalignment. The corrected BC signal (black), shifted by 160 seconds, shows alignment with vehicle activity.

3.3 Black Carbon Regressor Model

Table 1 presents the complete set of features extracted from our pipeline, consisting of vehicle emission covariates and environmental features. Our analysis, detailed in Section 5.2, further refines this set for model prediction. We also obtained environmental features, such as wind speed, temperature, and humidity, from publicly available APIs [48].

Our primary objective is to determine whether video-based generated characteristics can effectively predict BC concentrations, aligning with environmental air quality research findings that demonstrate the significance of vehicle emission covariates in BC pollution. We formulate this as a supervised learning problem because the BC measurements serve as ground truth labels to train a model that can directly map input features and BC concentration.

Our model uses the XGBoost algorithm [7] using 75% of the dataset, as summarized in Table 2. XGBoost is well known for its computational efficiency and model performance [13]. Its regularized gradient-boosting

Table 1: List of vehicular-based and environmental features for black carbon prediction.

Feature	Description
$TotalVehicle_t$	Count of all vehicles at time t
$LDPV_l$	Count of LDPV in lane l
HDV_l	Count of HDV in lane l
$StopLDPV_l$	Count of LDPVs stopped in lane l
$StopHDV_l$	Count of HDVs stopped in lane l
his_humid	Historical humidity (2 min prior, %)
his_temp	Historical temperature (2 min prior, °C)
his_wind	Historical wind speed (10 meter above the earth, km/s)

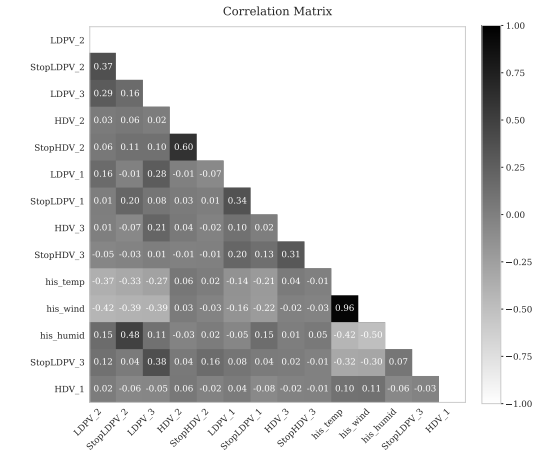


Figure 5: Correlation matrix. We excluded highly correlated features above 0.70.

framework builds trees sequentially to minimize training loss while controlling overfitting through shrinkage; after tuning, the best-performing hyperparameters were a learning rate (*learning_rate*) of 0.05, a maximum tree depth (*max_depth*) of 5, and 50 trees (*n_estimators*). It is trained on vehicle and environment features, and highly correlated features are excluded (see Figure 5).

4 Study

This study is approved by our university’s research ethics board. We collected traffic video and BC concentration data from three different streets in Downtown Toronto, a densely populated urban area with some of the worst traffic congestion globally [4]. Figure 6 illustrates three distinct street layouts from which the data were collected.

4.1 Data Collection System Setup

As illustrated in Figure 7, we designed a setup consisting of a microaethalometer sensor to measure BC concentration, a microphone to capture audio signals and a smartphone

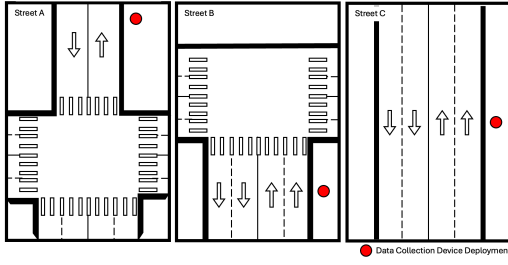


Figure 6: Three streets layouts for data collection.



Figure 7: Device setup for data collection.

camera to record video footage. This setup mimics the one used by Dawton *et al.* for roadside vehicle identification [8]. Separately, we developed an online data collection application (see Appendix Figure 22) using a combination of FastAPI for the server side and Jinja2 for templating on the client side. We integrated open-source APIs, including OpenMeteo and OpenStreetMap [29, 48]. For real-time traffic updates, we utilized the TomTom Traffic API [38]. This setup allowed our research team to configure custom data collection studies combining time periods, environmental conditions, and traffic variables for analysis.

4.2 Dataset

Table 2 summarizes the details of our dataset. It consists of short-term BC concentration measurements collected from four road junctions across different days, within a limited geographical area of our university. Thus, our data resulted in a highly constrained and heterogeneous sample size. With a total of 124 minutes, it is evidently too small to support a robust spatio-temporal evaluation. The constraint was dictated by logistical issues from loaning a microaethalometer within a restricted period, preventing an extensive and balanced data collection campaign.

The composition of vehicles was predominantly light duty in all sets, accounting for approximately 98% of the time, with HDVs constituting a minor fraction. Weather

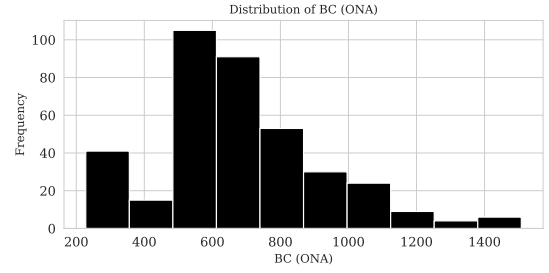


Figure 8: Distribution of BC ground truth readings from the microaethalometer after applying the Optimized Noise-Reduction Algorithm (ONA).

conditions varied throughout the study period, ranging from cloudy skies with strong winds to milder breezes and occasional snowfall. Wind speeds fluctuated between low and moderate, while humidity levels were predominantly in the moderate to high range, with periods of very high humidity. BC concentrations measured by the microaethalometer peaked at $1623\text{ng}/\text{m}^3$, with the lowest values attributed to device miscalibration. As per Figure 8, the average BC concentration was $685\text{ng}/\text{m}^3$, with a standard deviation of ± 249 after noise reduction.

5 System Evaluation

5.0.1 Objective. Our modeling objective is to evaluate how well vehicle-related features explain BC concentrations, rather than to demonstrate strong spatio-temporal generalization. Data from all four collection periods were combined before stratified sampling of 75% train and 25% test to achieve two aims. First, it ensures the model is trained on the full range of BC concentrations and traffic-related feature variations observed across all sites. Second, it allows the test set to evaluate the model’s ability to interpolate pollutant levels within the conditions already represented in the data. As a supplementary evaluation, we consider a windowed stratified split that respects the temporal ordering within each dataset by grouping samples into a fixed-length time window of 15 minutes. This ensures that all samples within a window are kept together and that training data precedes test data within each dataset. The added approach helps shed light on temporally subsequent observations. In our experiments, we removed outliers from the training data, but the test set remained unchanged.

5.0.2 Performance Metric. Models are evaluated using R^2 , Mean Absolute Error (MAE), and Root Mean Squared Error (RMSE). While R^2 measures variability capture and MAE provides average error magnitude, we prioritize RMSE as the primary metric because it provides a more interpretable

Table 2: Summary of data collected.

	Location	Duration	LDPV	HDV	Wind	Humidity	BC (in ng/m^3)
Set_A	Lat: 43.658 Lon: -79.395	49.0 mins	97.4%, $n=736$	2.6%, $n=20$	$\mu=15.59$, $\sigma=0.10$, min=15.5, max=15.7	$\mu=68.86$, $\sigma=0.99$, min=68.0, max=70.0	$\mu=828.03$, $\sigma=219.51$, min=427, max=1508
Set_B	Lat: 43.660 Lon: -79.397	32.5 mins	95.1%, $n=442$	4.9%, $n=23$	$\mu=27.03$, $\sigma=1.57$, min=24.5, max=28.0	$\mu=66.28$, $\sigma=0.45$, min=66.0, max=67.0	$\mu=729.82$, $\sigma=260$, min=-242, max=1623
Set_C	Lat: 43.659 Lon: -79.393	32.5 mins	99.5%, $n=551$	0.5%, $n=3$	$\mu=5.70$, $\sigma=0.69$, min=4.9, max=6.3	$\mu=67.29$, $\sigma=1.49$, min=66.0, max=69.0	$\mu=391$, $\sigma=191$, min=93, max=973
Set_D	Lat: 43.659 Lon: -79.394	10.0 mins	100%, $n=90$	0%, $n=0$	$\mu=9.20$, $\sigma=0.00$, min=9.2, max=9.2	$\mu=78.00$, $\sigma=0.00$, min=78.0, max=78.0	$\mu=502$, $\sigma=269$, min=167, max=1391

measure of predictive error, penalizes large errors and remains in the target unit of ng/m^3 .

Table 3: Model evaluation using different algorithms. XGBoost regression yields the best performance.

	Train RMSE / MAE / R^2	Test RMSE / MAE / R^2	p
LR (baseline)	184.70 / 146.83 / 0.34	211.66 / 163.56 / 0.25	-
SVR	216.20 / 155.23 / 0.10	238.49 / 170.78 / 0.05	$p > .01$
RF	82.71 / 62.01 / 0.87	131.86 / 91.70 / 0.71	$p < .001$
GB	77.31 / 58.15 / 0.88	136.76 / 93.53 / 0.68	$p < .001$
XGBoost	95.68 / 71.57 / 0.82	129.42 / 91.11 / 0.72	$p < .001$
XGBoost (windowed)	82.25 / 51.88 / 0.91	119.93 / 93.25 / 0.30	$p < .001$

Table 4: XGBoost regression yields best performance with Optimized Noise-Reduction Algorithm (ONA) and removing outliers locally in each dataset.

	Train RMSE / MAE / R^2	Test RMSE / MAE / R^2	p
None (baseline)	158.93 / 123.52 / 0.67	212.47 / 158.42 / 0.49	-
ONA	121.83 / 86.40 / 0.76	140.10 / 99.43 / 0.67	$p > .05$
Trim (global)	137.27 / 111.46 / 0.65	210.78 / 153.43 / 0.50	$p > .1$
Trim (local)	111.02 / 84.04 / 0.79	207.22 / 144.58 / 0.52	$p > .05$
ONA+Trim (global)	75.25 / 56.72 / 0.88	135.57 / 94.20 / 0.69	$p < .05$
ONA+Trim (local)	95.68 / 71.57 / 0.82	129.42 / 91.11 / 0.72	$p < .05$

5.1 Results

5.1.1 Model Selection. Table 3 summarizes the model performance for both our training and testing. We treated Linear Regression as the baseline given its simplicity and effectiveness in providing model interpretability. Where the RMSE value closer to zero and R^2 closer to 1 is most ideal, our experiments found that the XGBoost regression performs best. The overall regression is statistically significant ($R^2=0.72$, $p<.001$) compared to employing Linear Regression, but it is not significantly different from a

Random Forest regressor and Gradient Boosting. Figure 9 plots BC ground truth data against model predictions in our test set, with the results deviating from the true value by approximately $129.42ng/m^3$. When temporal structure is enforced using windowed stratified split, the R^2 (0.30, $p<.001$) decreases as expected due to limited temporal depth in each set. However, it is notable that RMSE and MAE remain within a comparable range ($119.93ng/m^3$, 91.11). Furthermore, 5-fold cross-validation on the training data yields an R^2 of 0.91, indicating that the model explains a large proportion of variance on unseen data drawn from the same temporal distribution as the training data.

5.1.2 Noise Reduction. Since BC readings obtained from aethalometers are often subject to noise, we employed noise reduction strategies as per Section 3.2.1. In removing outliers, the test set remained completely unchanged. Table 4 summarizes the model performance across different approaches. Applying the ONA method is evidently a significant step in improving our model's performance, boosting the R^2 value from 0.49 to 0.62. Given that our data sets were collected at different traffic junctions, removing outliers locally in each set before combining allows natural traffic variation to be preserved and ensures that the outlier removal process is appropriate for each context. When comparing global and local trimming with baseline, we found that local trimming yielded better results, but these differences are statistically insignificant. Finally, combining ONA with local trimming emerges as the most effective approach, offering the best overall performance at $p<.05$.

5.2 Features per Case-based Analysis

We employed SHAP (SHapley Additive ExPlanations) analysis, a game-theoretic approach that assigns each feature a contribution value for individual predictions [23]. Although the R^2 values differ substantially between our evaluation schemes, both approaches identify a similar set of features as the strongest contributors, as per Figure 10. The dominant predictors reflect stable relationships between vehicle-related features and BC concentration that do not depend strongly on how data was partitioned.

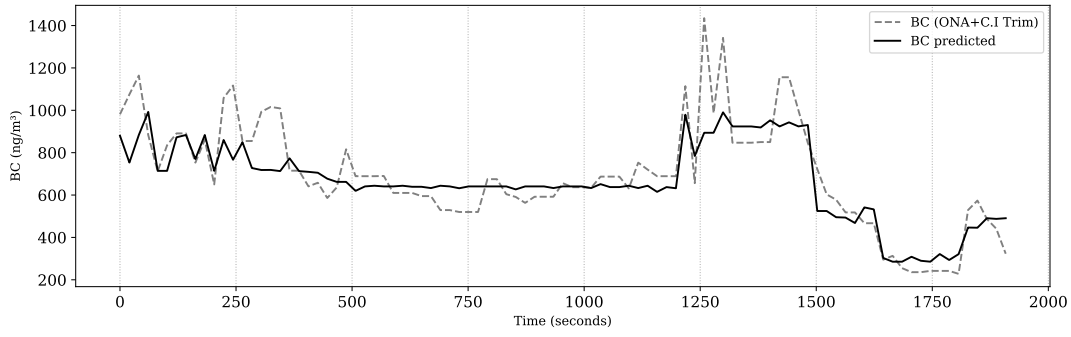


Figure 9: Predicted BC concentration (black) compared against ground truth BC data (dotted) on test set.

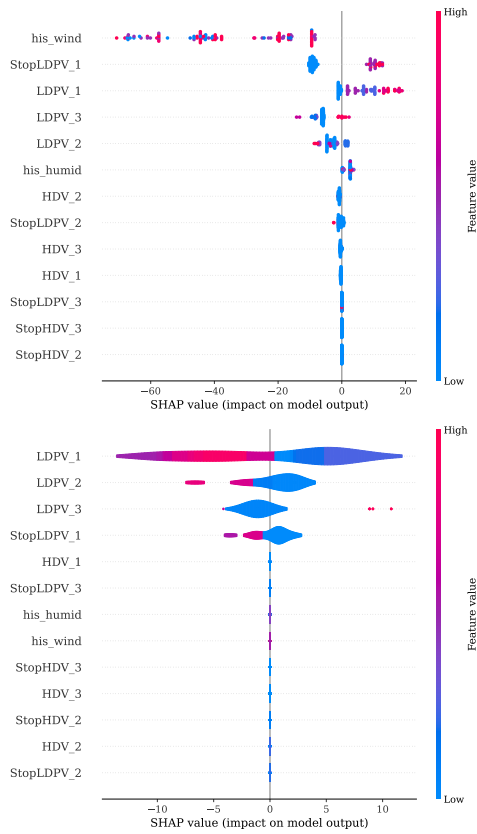


Figure 10: SHAP analysis for stratified (top) and windowed stratified (bottom) shows strong similarities.

To better understand the inner workings of the model, we visualize the prediction outcomes in Figure 11. In this plot, gray points represent predictions with smaller errors (those with a prediction error below the mean RMSE), while black points highlight the worst-case predictions, where the error exceeds the mean RMSE. Notably, the plot illustrates a clear

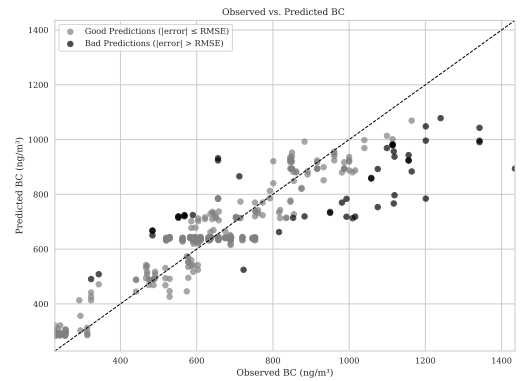


Figure 11: Prediction outcomes with smaller errors are defined as those with an error lower than the mean RMSE. Black points represent the worst-case errors, with increasing trend in high-BC scenarios.

trend of our model performance deteriorating at higher BC concentrations. This result suggests an increased difficulty in prediction in high-BC scenarios, which we conjecture to be influenced by environmental factors.

5.2.1 Impact of Environmental Factors. As per Figure 10 (top), wind speed (*his_wind*) consistently emerged as the strongest predictor. This aligns with previous studies, which have repeatedly suggested that moderate wind speeds facilitate pollutant dispersion while lower wind speeds influence BC deposition [17, 41]. In further examining our predicted outcomes, we found larger prediction errors associated with conditions of low wind speed (70%), as per Figure 12. The difference between good and bad predictions at low wind speed is statistically significant ($p < .001$).

Humidity (i.e., *his_humid*) is less influential compared to other vehicle emission factor covariates that contribute more significantly to the variation in BC concentrations. As per Figure 13, both good and bad predictions were generally associated with low humidity. However, there were more

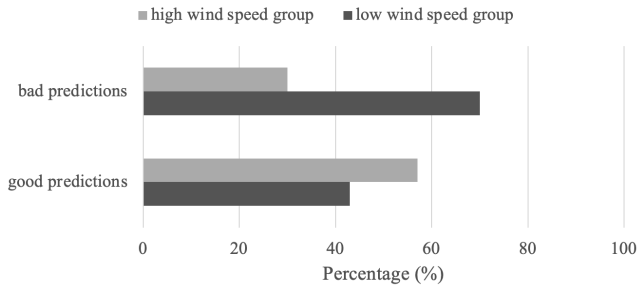


Figure 12: Distribution of predictions shows bad predictions attributed to low wind speed than high.

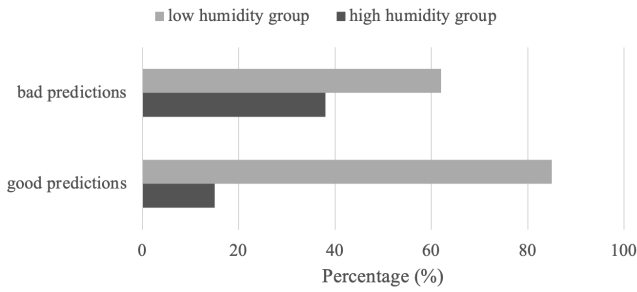


Figure 13: Distribution of predictions shows more bad predictions attributed to high humidity than low.

bad predictions associated with high humidity than good ones. This difference is statistically significant at $p < .005$. Both low wind speeds and high humidity can significantly influence BC concentrations in the air. Under low wind speeds, the atmosphere is less ventilated, meaning that pollutants such as BC are less likely to disperse and can accumulate near the ground [17]. High humidity can also affect BC concentrations by influencing their physical properties and affecting how they interact with atmospheric processes such as deposition. The combination of these factors creates complex environmental conditions in which predicting BC levels becomes increasingly challenging.

5.2.2 Impact of Vehicle-based Covariates: Best Case. With the strongest features associated with the acceleration of passenger vehicles after a full stop and their being in the lane of the road closest to our monitoring setup (i.e., $StopLDPV_1$), we visualized the predicted BC values against the ground truth, overlaying corresponding vehicle counts for both moving and stopped LDPV and HDVs in all lanes, as per Figure 14. Our observations support the claim that stopped vehicles (and, as a result, their acceleration) have a disproportionately large effect on BC concentration [10, 46]. In scenarios where stopped vehicles were present among moving LDPVs, predicted BC concentrations were

consistently higher compared to periods of continuous, free-flowing traffic. This result underscores the increased influence of idle or stop-and-go traffic near the monitoring location, likely due to the accumulation of localized emissions and the reduced dispersion under stationary conditions. For example, the highest peak in BC concentration at t_3 corresponds to localized emission surges of 5 stopped and 10 moving LDPVs.

5.2.3 Impact of Vehicle-based Covariates: Worst Case. Figure 15 charts our worst-case scenario in which the prediction error exceeds the average margin of $\pm 245 \text{ ng/m}^3$. We identified two sources of inaccuracy from the raw data logs. The first limitation arises from the small amount of training data available for HDVs. As a result, the model produced errors at t_7 , t_{13} , and t_{14} , where higher BC concentrations were observed due to the passage of HDVs that were not adequately represented in training. Consistent with this, the SHAP analysis ranked HDV-related characteristics less important, despite strong evidence that such vehicles emit substantially more BC than LDPVs [46, 47]. The second limitation stems from object occlusion in our video data. Along this roadway, a streetcar operates in mixed traffic. Although the streetcar itself is electric and does not emit BC, its presence forces surrounding vehicles to stop and then accelerate once it is safe to move again. These stop-start conditions generate substantial amounts of BC. However, our technique was unable to fully capture them because the streetcar occluded many of the stopped vehicles and led to undercounting of vehicle types and misclassification of stopping and acceleration events.

After excluding the affected data points, model performance improved, with RMSE decreasing to 114 ng/m^3 . Ground-level video surveillance often suffers from object occlusion, and this effect would be mitigated in datasets captured from aerial or elevated camera angles.

Key Takeaway: Our BC prediction model integrates emission-related covariates derived from traffic video recordings with environmental variables extracted from daily weather data. Using an XGBoost regression framework, the model achieved an R^2 of 0.72 and an RMSE of $129.42 \text{ (ng/m}^3\text{)}$. This result indicates that 72% of the variance in BC levels can be explained by the selected features. The corresponding MAE increased only modestly from 71 (train) to 91 (test), suggesting limited overfitting and that the model generalizes reasonably well to unseen data within the available dataset. Patterns of stop-and-accelerate behavior, particularly for vehicles in the lane closest to the monitoring setup, align with established findings in the literature. What is novel here is that these patterns are derived from computer vision features,

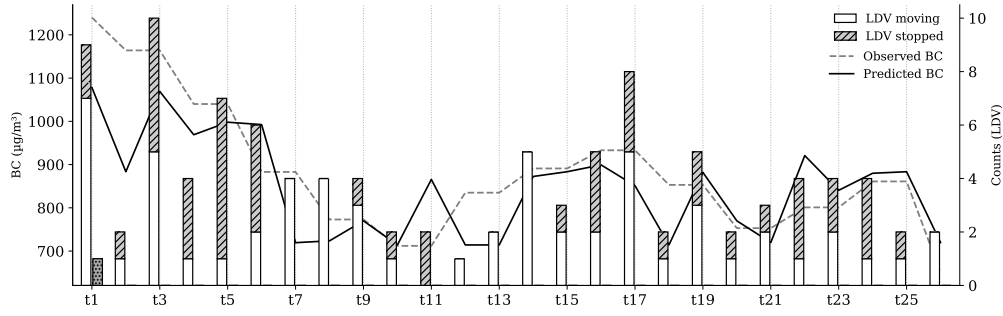


Figure 14: Predicted and observed BC concentrations, combined with counts of moving and stopped LDPVs and HDVs over 13 minutes. Predicted values follow the general trend of surges in stopped and moving traffic.

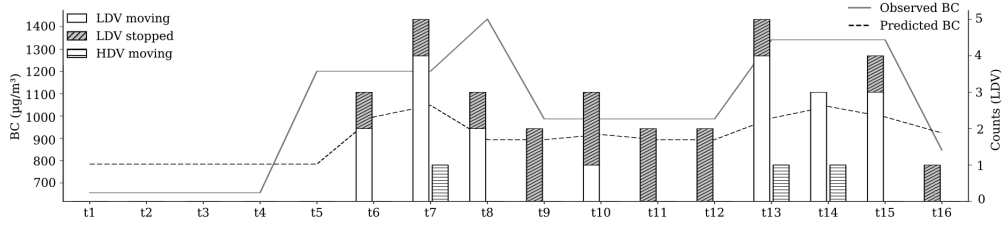


Figure 15: Predicted and observed BC concentrations, combined with counts of vehicles. Predicted values do not follow the general trend of observed BC concentration, but aligns with vehicle presence.

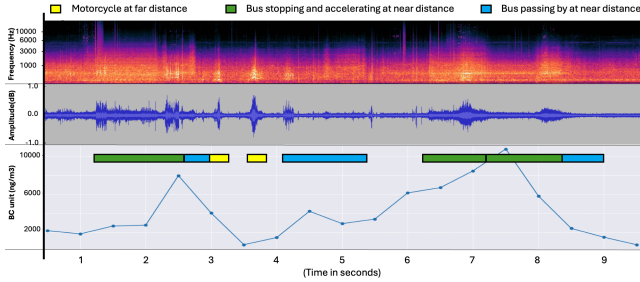


Figure 16: Spectrogram (top) and waveform (middle) show audio differences across bus states; bottom panel shows corresponding BC levels.

demonstrating the potential of vision-based approaches to capture real-world emission dynamics.

6 Discussion

We proposed a CV-based method to estimate the amounts of BC concentration in traffic using traffic video recordings as a primary data source. Here, we discuss the limitations and implications of our findings.

6.1 Improving Model Performance

This study focuses on the use of CV techniques to extract standard vehicle characteristics. However, our model implementation has limitations, particularly in training one that differentiates green vehicles from conventional vehicles. Other techniques can be extended. For instance, license plate detection can reveal codes of fuel type, as in Ontario, Canada, where plates beginning with “GV” are designated for green vehicles. In practice, this implementation means extracting only the minimal information required, while avoiding the storage of full license plate data or allowing the data to be repurposed for other uses.

Beyond vision-based cues, acoustic sensing holds promise for distinguishing engine types, and our work continues to examine how audio signals [8] can be integrated. We are currently extending audio-sensing capabilities, as per prior work [26, 44], extracting features such as zero crossing rate, root mean square energy, spectral roll-off, and spectral centroid. As illustrated in Figure 16, we observed clear peaks in BC concentration shortly after the presence of buses near our audio-sensing prototype.

We anticipate continuous audio monitoring along congested highways to be overwhelming and largely impractical due to background noise and traffic volume, but targeted deployment in community zones can still provide meaningful value.

6.2 Monitoring for Environmental Justice

Environmental justice research on BC and ultrafine particles (UFPs) remains relatively limited in general, but urban research in Canada and the US has highlighted emerging concerns [4, 6]. Specifically, as an example, Elford *et al.* reported that areas in Toronto with a higher prevalence of immigrants faced greater exposure to UFPs during walks to school [12], supporting broader findings from U.S. cities where low-income and visible minority groups, particularly Black, Hispanic and Latino populations, are disproportionately exposed to high BC concentrations [6]. Our study is geographically limited to several streets in the Downtown Toronto region, where traffic is predominantly dense. While the current dataset does not capture seasonal variations, it does include variation in wind speed, which is highly relevant for BC prediction. Our experiments demonstrated the technical feasibility through strong correlations between video-derived vehicle inferences and BC concentration. At the same time, these results provided us with clearer guidance in conducting a long-term regional study, including additional sensing tools that we will now consider to improve prediction.

Unlike regulatory weather stations or low-cost air quality sensors, which are often more prevalent in predominantly white and higher income neighborhoods [20], traffic surveillance cameras tend to be more available in urban environments. This availability makes traffic surveillance cameras a useful data source for near-source BC estimation from traffic. While the disproportionate placement of traffic surveillance cameras in lower-income communities has raised equity concerns [27], this existing infrastructure could be leveraged for positive purposes. Instead of reinforcing punitive or enforcement-heavy practices, traffic cameras can support environmental and public health monitoring by providing insight into traffic pollution and guiding interventions that benefit the very communities most affected. Furthermore, BC concentrations are influenced by broader urban and regional environmental factors, including local topography and contributions from other sources such as wildfires, industrial emissions, and residential heating. Hence, weather stations equipped with microaethalometers remain the gold standard for capturing complex regional and atmospheric dynamics. Instead, our system focuses on near-source estimations of street-level traffic, complementing research-grade instruments.

From a policy perspective, having more localized BC estimates plays a critical role in strengthening the evidence base for environmental justice efforts. Beyond identifying areas of concern, such data can directly inform targeted interventions, including reducing vehicle idle near traffic hotspots and school zones, redirecting HDVs away from

residential neighborhoods during peak pedestrian hours, and optimizing traffic signal timing in areas with frequent peaks of stopped vehicles [45].

7 Conclusion

Traffic video recordings are a valuable resource for transportation planning, public safety, and urban development. While ML-driven applications in this domain have largely focused on improving driver behavior and enabling dynamic traffic management, their potential to study the environmental impacts of traffic remains underexplored. This gap is especially critical given the urgent need to address pollution in urban environments, where traffic is a major source of BC emissions. However, the subject of BC is particularly challenging to study due to the high cost and complexity of instrumentation and gathering measurements compared to other pollutants. We proposed an ML-driven approach that determines vehicle emission factor covariates to estimate BC concentration. Our XGBoost regression model achieved an R^2 of 0.72 and an RMSE of 129.42 ng/m^3 . Modeling BC concentration prediction is inherently constrained from reaching an R^2 close to 1 because these pollutants are influenced not only by this source but also by regional factors (e.g., in nearby towns), urban structures, and other local sources (e.g., residential exhaust). Since our approach focuses only on vehicle-related local factors, an R^2 of 0.72 is a promising outcome, reflecting the natural but partial scope of predictors. The most influential predictors identified were wind speed, vehicle acceleration after stopping, and the distance between the vehicle and the measurement device. These findings align with prior research showing that wind speed affects pollutant dispersion, with BC concentrations highest near sources and decreasing with distance. Our work continues with a larger data collection campaign spanning the Greater Toronto Area across seasonal changes, expanding video coverage and incorporating audio.

Acknowledgments

This work is supported by the Natural Sciences and Engineering Research Council of Canada. [RGPIN-2025-06914]

References

- [1] Mian Ahmad Jan, Muhammad Adil, Bouziane Brik, Saad Harous, and Sohail Abbas. 2025. Making Sense of Big Data in Intelligent Transportation Systems: Current Trends, Challenges and Future Directions. *Comput. Surveys* 57, 8 (2025), 1–43.
- [2] UN General Assembly et al. 2015. Transforming our world: the 2030 Agenda for Sustainable Development. (2015).
- [3] George A Ban-Weiss, Melissa M Lunden, Thomas W Kirchstetter, and Robert A Harley. 2009. Measurement of black carbon and particle number emission factors from individual heavy-duty trucks.

- Environmental Science & Technology* 43, 4 (2009), 1419–1424. doi:10.1021/es8021039
- [4] Emmanuelle Batisse, Marshall Lloyd, Alicia Cavanaugh, Arman Ganji, Junshi Xu, Marianne Hatzopoulou, Jill Baumgartner, and Scott Weichenthal. 2025. Examining the social distributions in neighbourhood black carbon and ultrafine particles in Montreal and Toronto, Canada. *Environment International* 198 (2025), 109395.
 - [5] Thomas L Brewer. 2017. Black carbon problems in transportation: Technological solutions and governmental policy solutions. In *Proceedings of the MIT CEEPR Conference, Paris, France*, Vol. 7.
 - [6] Sarah E Chambliss, Carlos PR Pinon, Kyle P Messier, Brian LaFranchi, Crystal Romeo Upperman, Melissa M Lunden, Allen L Robinson, Julian D Marshall, and Joshua S Apte. 2021. Local-and regional-scale racial and ethnic disparities in air pollution determined by long-term mobile monitoring. *Proceedings of the National Academy of Sciences* 118, 37 (2021), e2109249118.
 - [7] Tianqi Chen and Carlos Guestrin. 2016. Xgboost: A scalable tree boosting system. In *Proceedings of the 22nd acm sigkdd international conference on knowledge discovery and data mining*. 785–794.
 - [8] Billy Dawton, Shigemi Ishida, Yuki Hori, Masato Uchino, Yutaka Arakawa, Shigeaki Tagashira, and Akira Fukuda. 2020. Initial evaluation of vehicle type identification using roadside stereo microphones. In *2020 IEEE Sensors Applications Symposium (SAS)*. IEEE, 1–6.
 - [9] Priyanka Desouza and Patrick L Kinney. 2021. On the distribution of low-cost PM_{2.5} sensors in the US: demographic and air quality associations. *Journal of exposure science & environmental epidemiology* 31, 3 (2021), 514–524.
 - [10] Evi Dons, Philip Temmerman, Martine Van Poppel, Tom Bellemans, Geert Wets, and Luc Int Panis. 2013. Street characteristics and traffic factors determining road users' exposure to black carbon. *Science of the Total Environment* 447 (2013), 72–79.
 - [11] Richard O. Duda and Peter E. Hart. 1972. Use of the Hough Transformation to Detect Lines and Curves in Pictures. *Commun. ACM* 15, 1 (1972), 11–15. doi:10.1145/361237.361242
 - [12] Spencer Elford and Matthew D Adams. 2021. Associations between socioeconomic status and ultrafine particulate exposure in the school commute: An environmental inequality study for Toronto, Canada. *Environmental Research* 192 (2021), 110224.
 - [13] M Ester, HP Kriegel, and XJGA Xu. 2022. XGBoost: A scalable tree boosting system. In *Proceedings of the 22Nd ACM SIGKDD International Conference on Knowledge Discovery and Data Mining* (vol. pg 785, 2016). *GEOGRAPHICAL ANALYSIS* (2022).
 - [14] Government of Canada. 2025. Black Carbon Emissions Inventory: overview. <https://www.canada.ca/en/environment-climate-change/services/pollutants/black-carbon-emissions-inventory.html>. Accessed: 27 April 2025.
 - [15] Örjan Gustafsson and Veerabhadran Ramanathan. 2016. Convergence on climate warming by black carbon aerosols. *Proceedings of the National Academy of Sciences* 113, 16 (2016), 4243–4245.
 - [16] Gayle SW Hagler, Tiffany LB Yelverton, Ram Vedantham, Anthony DA Hansen, and Jay R Turner. 2011. Post-processing method to reduce noise while preserving high time resolution in aethalometer real-time black carbon data. *Aerosol and Air Quality Research* 11, 5 (2011), 539–546.
 - [17] Nathan Hilker, Jonathan M Wang, Cheol-Heon Jeong, Robert M Healy, Uwayemi Sofowote, Jerzy Deboasz, Yushan Su, Michael Noble, Anthony Munoz, Geoff Doerksen, et al. 2019. Traffic-related air pollution near roadways: discerning local impacts from background. *Atmospheric Measurement Techniques* 12, 10 (2019), 5247–5261.
 - [18] Shuai Hua, Manika Kapoor, and David C Anastasiu. 2018. Vehicle tracking and speed estimation from traffic videos. In *Proceedings of the IEEE Conference on Computer Vision and Pattern Recognition Workshops*. 153–160.
 - [19] Weaam Jaafar, Jad Zalzal, Junshi Xu, Arman Ganji, and Marianne Hatzopoulou. 2025. Refining Air Pollution Exposure Estimates: A Comparison of Citywide and Neighborhood Land Use Regression Models in Toronto. *Environmental Science & Technology* (2025).
 - [20] Makoto M Kelp, Timothy C Fargiano, Samuel Lin, Tianjia Liu, Jay R Turner, J Nathan Kutz, and Loretta J Mickley. 2023. Data-driven placement of PM_{2.5} air quality sensors in the United States: An approach to target urban environmental injustice. *Geohealth* 7, 9 (2023).
 - [21] Patricia Krecl, Yago Alonso Cipoli, Admir Créso Targino, Matheus de Oliveira Toloto, David Segerström, Álvaro Parra, Gabriela Polezer, Ricardo Henrique Moreton Godoi, and Lars Gidhagen. 2019. Modelling urban cyclists' exposure to black carbon particles using high spatiotemporal data: A statistical approach. *Science of the Total Environment* 679 (2019), 115–125.
 - [22] Min Liu, Xia Peng, Ziqi Meng, Taoye Zhou, Lingbo Long, and Qiannan She. 2019. Spatial characteristics and determinants of in-traffic black carbon in Shanghai, China: Combination of mobile monitoring and land use regression model. *Science of the Total Environment* 658 (2019), 51–61.
 - [23] Scott M Lundberg and Su-In Lee. 2017. A unified approach to interpreting model predictions. *Advances in neural information processing systems* 30 (2017).
 - [24] Kyle P Messier, Sarah E Chambliss, Shahzad Gani, Ramon Alvarez, Michael Brauer, Jonathan J Choi, Steven P Hamburg, Jules Kerckhoffs, Brian LaFranchi, Melissa M Lunden, et al. 2018. Mapping air pollution with Google Street View cars: Efficient approaches with mobile monitoring and land use regression. *Environmental science & technology* 52, 21 (2018), 12563–12572.
 - [25] Laura Minet, Rick Liu, Marie-France Valois, Junshi Xu, Scott Weichenthal, and Marianne Hatzopoulou. 2018. Development and comparison of air pollution exposure surfaces derived from on-road mobile monitoring and short-term stationary sidewalk measurements. *Environmental science & technology* 52, 6 (2018), 3512–3519.
 - [26] Jure Murovec, Jurij Prezelj, Dejan Čirić, and Marko Milivojević. 2024. Zero Crossing Signature: A Time-Domain Method Applied to Diesel and Gasoline Vehicle Classification. *IEEE Sensors Journal* (2024).
 - [27] Vision Zero Network. 2025. Making Speed Safety Cameras Effective & Fair: From Planning to Action. <https://visionzeronetWORK.org/promoting-equity-in-speed-safety-camera-programs-from-planning-to-action/>. Accessed: 2025-09-09.
 - [28] Amanda L Northcross, Shizuka Hsieh, Sacoby Wilson, Ebony Roper, Russell R Dickerson, Parisa Norouzi, and Vernon Morris. 2020. Monitoring neighborhood concentrations of PM_{2.5} and black carbon: When using citywide averages underestimates impacts in a community with environmental justice issues. *Environmental Justice* 13, 2 (2020), 27–35.
 - [29] OpenStreetMap contributors. 2017. Planet dump retrieved from <https://planet.osm.org>. <https://www.openstreetmap.org>.
 - [30] Fatema Parvez and Kristina Wagstrom. 2019. A hybrid modeling framework to estimate pollutant concentrations and exposures in near road environments. *Science of the Total Environment* 663 (2019), 144–153.
 - [31] Kun Qian, Shilin Zhu, Xinyu Zhang, and Li Erran Li. 2021. Robust multimodal vehicle detection in foggy weather using complementary lidar and radar signals. In *Proceedings of the IEEE/CVF Conference on Computer Vision and Pattern Recognition*. 444–453.
 - [32] Milad Saeedi, Junshi Xu, Usman Ahmed, Matthew Roorda, and Marianne Hatzopoulou. 2025. Urban Air Pollution Data Collection, Mapping, and Prediction Using Mobile Sensors Installed on Courier

- Trucks. *Transportation Research Record* (2025), 03611981251324208.
- [33] Haley Samsel. 2019. Study: One Billion Surveillance Cameras Expected to Be Installed Globally By 2021. *Security Today* (Dec. 09 2019). <https://securitytoday.com/articles/2019/12/09/one-billion-surveillance-cameras-expected.aspx> Accessed: YYYY-MM-DD.
- [34] Marjan Savadkoobi, Marco Pandolfi, Cristina Reche, Jarkko V Niemi, Dennis Mooibroek, Gloria Titos, David C Green, Anja H Tremper, Christoph Hueglin, Eleni Liakakou, et al. 2023. The variability of mass concentrations and source apportionment analysis of equivalent black carbon across urban Europe. *Environment international* 178 (2023), 108081.
- [35] Young Sunwoo. 2025. Why measuring black carbon is key to climate change mitigation. World Economic Forum, Centre for Nature and Climate. <https://www.weforum.org/stories/2025/02/why-measuring-black-carbon-is-key-to-climate-change-mitigation/>
- [36] Stacey Sutton and Nebiyu Tilahun. 2022. *Red-Light and Speed Cameras: Analyzing the Equity and Efficacy of Chicago's Automated Camera Enforcement Program – Executive Summary*. Executive Summary. University of Illinois Chicago, Chicago, IL. https://www.chicago.gov/content/dam/city/depts/cdot/Red%20Light%20Cameras/2022/Sutton+Tilahun_Chicago-Camera-Ticket_Exec%20Summary-Final-Jan10.pdf Submitted to the City of Chicago Mayor's Office and Department of Transportation.
- [37] Hoda Talaat, Junshi Xu, Marianne Hatzopoulou, and Hossam Abdelgawad. 2021. Mobile monitoring and spatial prediction of black carbon in Cairo, Egypt. *Environmental Monitoring and Assessment* 193, 9 (2021), 587.
- [38] TomTom International BV. 2025. TomTom Traffic API Documentation. <https://developer.tomtom.com/traffic-api/traffic-api-documentation>. Accessed: 27 April 2025.
- [39] Sara Torbatian, Marc Saleh, Junshi Xu, Laura Minet, Shayamila Mahagammulla Gamage, Daniel Yazgi, Shoma Yamanouchi, Matthew J Roorda, and Marianne Hatzopoulou. 2024. Societal co-benefits of zero-emission vehicles in the freight industry. *Environmental Science & Technology* 58, 18 (2024), 7814–7825.
- [40] Rejin Varghese and M Sambath. 2024. Yolov8: A novel object detection algorithm with enhanced performance and robustness. In *2024 International Conference on Advances in Data Engineering and Intelligent Computing Systems (ADICS)*. IEEE, 1–6.
- [41] Scott Weichenthal, William Farrell, Mark Goldberg, Lawrence Joseph, and Marianne Hatzopoulou. 2014. Characterizing the impact of traffic and the built environment on near-road ultrafine particle and black carbon concentrations. *Environmental research* 132 (2014), 305–310.
- [42] Scott Weichenthal, Marshall Lloyd, Arman Ganji, Leora Simon, Junshi Xu, Alessya Venuta, Alexandra Schmidt, Joshua Apte, Hong Chen, Eric Lavigne, et al. 2024. Long-Term Exposure to Outdoor Ultrafine Particles and Black Carbon and Effects on Mortality in Montreal and Toronto, Canada. *Research Reports: Health Effects Institute* 2024 (2024), 217.
- [43] Scott Weichenthal, Keith Van Ryswyk, Alon Goldstein, Scott Bagg, Maryam Shekharizfard, and Marianne Hatzopoulou. 2016. A land use regression model for ambient ultrafine particles in Montreal, Canada: A comparison of linear regression and a machine learning approach. *Environmental research* 146 (2016), 65–72.
- [44] Alicja Wiczorkowska, Elżbieta Kubera, Tomasz Słowik, and Krzysztof Skrzypiec. 2018. Spectral features for audio based vehicle and engine classification. *Journal of Intelligent Information Systems* 50, 2 (2018), 265–290.
- [45] Jad Zalzal and Marianne Hatzopoulou. 2022. Fifteen years of community exposure to heavy-duty emissions: capturing disparities over space and time. *Environmental Science & Technology* 56, 23 (2022), 16621–16632.
- [46] Shaojun Zhang, Ye Wu, Hao Yan, Xiaoyan Du, and K Max Zhang. 2019. Black carbon pollution for a major road in Beijing: Implications for policy interventions of the heavy-duty truck fleet. *Transportation Research Part D: Transport and Environment* 67 (2019), 237–246. doi:10.1016/j.trd.2018.11.013
- [47] Xuan Zheng, Shaojun Zhang, Ye Wu, K Max Zhang, Xian Wu, Zhenhua Li, and Jiming Hao. 2017. Characteristics of black carbon emissions from in-use light-duty passenger vehicles. *Environmental Pollution* 231 (2017), 348–356.
- [48] Patrick Zippenfenig. 2023. *Open-Meteo.com Weather API*. doi:10.5281/zenodo.7970649

A Dataset Excerpt

This appendix describes the raw and processed dataset we used for the experiments in this paper.

```

1 Date,Time,Ref,Sen,ATN,Flow,Pcb temp,Status,Battery,BC,Ona_#_pts_avg
2 2024/11/04,18:49:00,890665,921559,-3.40984263756,100,19,0,98,,NULL
3 2024/11/04,18:49:30,890783,921490,-3.3891073947402,99,19,0,98,2379,3
4 2024/11/04,18:50:00,890907,921527,-3.3792031816136,99,19,0,98,1136,3
5 2024/11/04,18:50:30,890941,921473,-3.369526908093,100,19,0,98,1099,3
6 2024/11/04,18:51:00,891037,921486,-3.3601631390269,100,19,0,98,1064,2
7

```

Figure 17: Raw data samples collected using the microaethalometer, microAeth AE51, collected at 30 seconds interval in .CSV

```

1 car_line1 : 2771 2024-11-05 17:23:02
2 car_line1 : 2775 2024-11-05 17:23:03
3 car_line2 : 2790 2024-11-05 17:23:05
4 truck_line2 : 2777 2024-11-05 17:23:07
5 person_line1 : 2785 2024-11-05 17:23:09
6 bicycle_line1 : 2795 2024-11-05 17:23:09
7

```

Figure 18: Features of vehicles in traffic extracted from the video processing pipeline. When an object is first seen, the system assigns a unique ID (e.g., 2771) and records their respective lane and timestamp.

```

1 {
2   "Time": "2024-11-05 17:34:50",
3   "BC": 1202,
4   "BC post": 1114,
5   "car_line1": 1,
6   "car_line3": 3,
7   "truck_line2": 1,
8   "car_line2": 2,
9   "car_line1_stop": 0,
10  "truck_line2_stop": 0,
11  "truck_line3": 0,
12  "truck_line1": 0,
13  "traffic": 0.65,
14  "history_temperature": 19.1,
15  "history_wind_speed": 24.5,
16  "history_humidity": 67,
17  "forecast_temperature": 18.7,
18  "forecast_wind_speed": 9.9,
19  "forecast_humidity": 68
20 }
21

```

Figure 19: This is an example row of what our final dataset looks like. The variable “BC post” indicates BC after applying Optimized Noise-Reduction Algorithm (ONA).

B Hyperparameter Tuning

We tuned model hyperparameters using cross-validated grid search in `scikit-learn`. Each model was wrapped in a common Pipeline so that parameters are referenced with the double-underscore convention, for example `model__max_depth`. The search spaces mirror the configuration used in our code.

Model	Parameter	Values
LinearRegression	(none)	No hyperparameters tuned
	<code>model__min_samples_split</code>	[2, 5]
RandomForestRegressor	<code>model__n_estimators</code>	[30, 50, 100, 200]
	<code>model__max_depth</code>	[None, 5, 6, 7, 9, 10]
	<code>model__n_estimators</code>	[20, 50, 100, 200, 250]
GradientBoostingRegressor	<code>model__learning_rate</code>	[0.01, 0.05, 0.1, 0.2]
	<code>model__max_depth</code>	[3, 5, 6, 7]
SVR	<code>model__C</code>	[0.1, 1, 10]
	<code>model__epsilon</code>	[0.01, 0.1, 1]
	<code>model__n_estimators</code>	[20, 50, 100, 200, 250]
XGBRegressor	<code>model__learning_rate</code>	[0.01, 0.05, 0.1, 0.2]
	<code>model__max_depth</code>	[3, 5, 6, 7]

We ran a cross-validated grid search per model and selected the configuration with the best mean validation score. Unless noted otherwise, we used five-fold cross-validation, refit the best configuration on the full training split, and reported scores on the held-out test split. A fixed `random_state` ensured repeatability.

- **RandomForestRegressor** tunes tree count (`n_estimators`), depth (`max_depth`), and split size (`min_samples_split`) to control ensemble capacity and variance.
- **GradientBoostingRegressor** balances `n_estimators` and `learning_rate`; `max_depth` limits individual tree depth.
- **SVR** primarily depends on `C` (regularization) and `epsilon` (tube width). We used the default RBF kernel unless specified.
- **XGBRegressor** varies `n_estimators`, `learning_rate`, and `max_depth` under the squared-error objective.

```

1  search = GridSearchCV(
2      estimator=pipe,                # e.g., Pipeline([('prep', ...), ('model', ...)])
3      param_grid=models[name]['params'],
4      scoring='neg_root_mean_squared_error',
5      cv=5, n_jobs=-1, refit=True
6  )
7  search.fit(X_train, y_train)
8  best_params = search.best_params_
9  cv_table    = search.cv_results_
10

```

Figure 20: Skeleton used for cross-validated grid search

C Database Schema for Dashboard

We use Docker Compose to start the dashboard and its services from a Compose file named `infrastructure.yaml`. The commands below assume you run them at the repository root.

```

1  # Bring services up (detached).
2  docker compose -f infrastructure.yaml up -d

```

```

1  # Check status.
2  docker compose -f infrastructure.yaml ps

```

```
1 # Stop and remove the stack.
2 docker compose -f infrastructure.yaml down
```

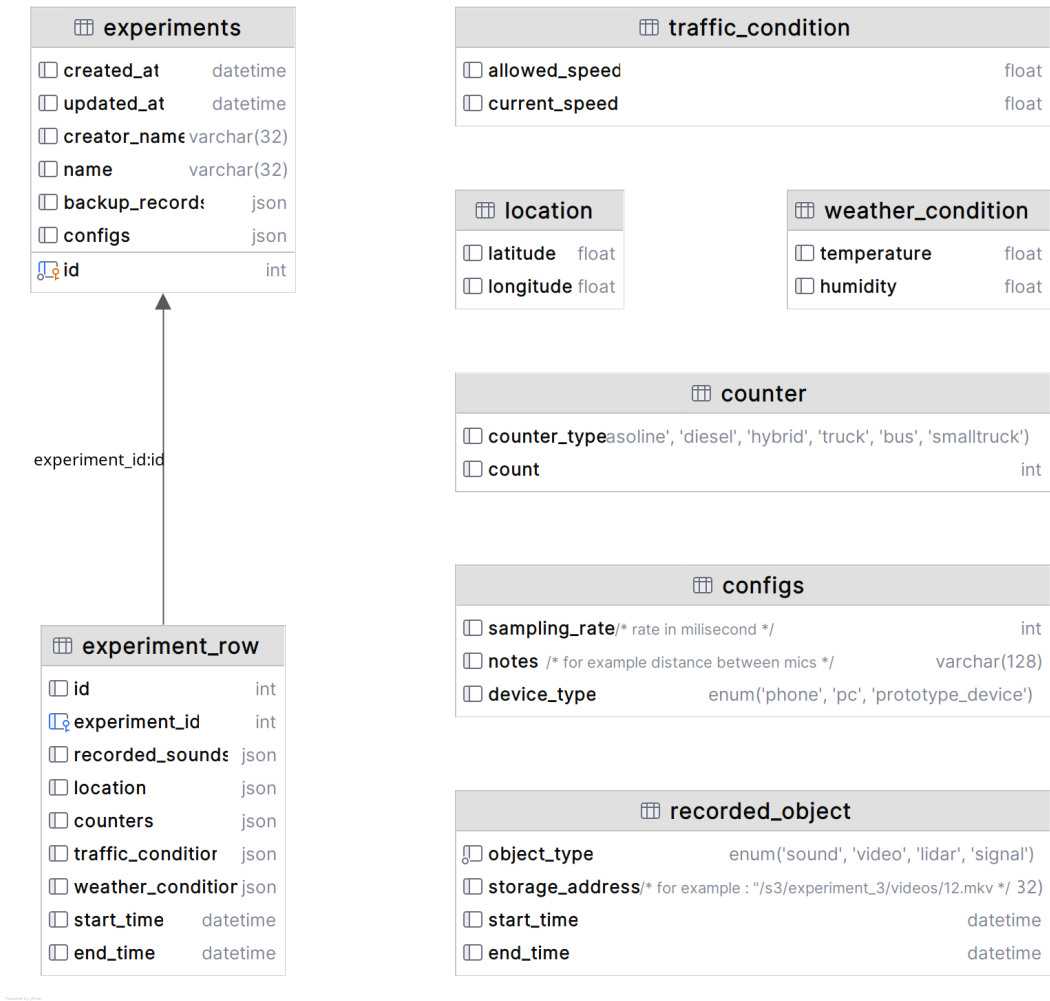


Figure 21: Database schema for our data collection dashboard.

New Experiment

Yonge Street 21 th

experiment_name

Yonge Street 21 th

creator_name

Aryan

sampling_rate

12

comment

User Experiment comment

sender_type

SenderType.HARDWARE

Run Experiment

9207 ms

latitude

43.6599240747891

longitude

-79.3906617164612

temperature °C

13.6

humidity %

67

wind_speed km/h

12



street allowed max speed

29

current_speed

29

traffic_condition

normal



gasoline

0

diesel

0

hybrid

0

truck

0

bus

0

small_truck

0

Experiment rows

id	start_time	end_time	location	humidity	wind_speed	temperature	traffic	gasoline	diesel	hybrid	truck	bus	small_truck	File
269	10/21/2024, 12:08:01 AM	10/21/2024, 12:08:13 AM	43.7485568, -79.331328	62	10	13.6	32 / 32	0	2	4	0	4	0	
270	10/21/2024, 12:08:13 AM	10/21/2024, 12:08:25 AM	43.7485568, -79.331328	62	10	13.6	32 / 32	4	0	7	9	0	0	

User input fields

Ground truth recording fields

Figure 22: Online dashboard consolidating data streams and manual observations into a structured format.